Preprint DFUB-91/5
27 May 1991

CM-P00063074

THE Λ_b^0 BEAUTY BARYON PRODUCTION IN PROTON-PROTON INTERACTIONS AT $\sqrt{s}$=62 GeV: A SECOND OBSERVATION

G. Bari, M. Basile, G. Bruni, G. Cara Romeo, R. Casaccia, L. Cifarelli, F. Cindolo, A. Contin, G. D'Alì, C. Del Papa, S. De Pasquale, P. Giusti, G. Iacobucci, G. Maccarrone, T. Massam, R. Nania, F. Palmonari, G. Sartorelli, G. Susinno, L. Votano and A. Zichichi

CERN, Geneva, Switzerland
Dipartimento di Fisica dell'Università, Bologna, Italy
Dipartimento di Fisica dell'Università, Cosenza, Italy
Istituto di Fisica dell'Università, Palermo, Italy
Istituto Nazionale di Fisica Nucleare, Bologna, Italy
Istituto Nazionale di Fisica Nucleare, LNF, Frascati, Italy

Abstract

Another decay mode of the Λ_b^0 (open-beauty baryon) state has been observed: $\Lambda_b^0 \to \Lambda_c^+\pi^+\pi^-\pi^-$. In addition, new results on the previously observed decay channel, $\Lambda_b^0 \to pD^0\pi^-$, are reported. These results confirm our previous findings on Λ_b^0 production at the ISR. The mass value (5.6 GeV/c^2) is found to be in good agreement with theoretical predictions. The production mechanism is found to be "leading".

(Submitted to Nuovo Cimento A)

1. INTRODUCTION

Experiment R422 was performed at the CERN-ISR in the last months of ISR operation as a proton-proton collider. The experiment was devoted to the study of charm and beauty (open-flavour) production in pp interactions at $\sqrt{s}$=62 GeV. The basic feature of the experiment was its capability to trigger on relatively high p_t single electrons and positrons. Baryonic heavy-flavoured states, hadronically decaying into charged particles, could be searched for in coincidence with electrons or positrons produced in the semileptonic decay of the associated heavy-flavoured antistates, via an invariant mass analysis.

In the present work we report the study of the reaction:

$$p + p \rightarrow e^+ + \Lambda_b^o + X \qquad (1)$$

where the Λ_b^o, i.e. the lightest beauty baryon with quark composition (udb), decays hadronically into two different final states:

$$\Lambda_b^o \rightarrow pD^o\pi^- \qquad (2)$$
$$\quad \hookrightarrow K^-\pi^+$$

$$\Lambda_b^o \rightarrow \Lambda_c^+\pi^+\pi^-\pi^- \qquad (3)$$
$$\quad \hookrightarrow pK^-\pi^+$$

and the e^+ originates from the semileptonic decay of the associated antibeauty-flavoured state, in the $\bar{b} \rightarrow \bar{c}$ transition.

The characteristics of the experiment in terms of set-up, trigger, data taking, and electron (positron) filtering, for a powerful lepton versus hadron selection, are briefly summarized. The whole invariant mass analysis, with the "forward" phase-space region explored for "leading" heavy baryon production, is described in detail. The Λ_b^o mass is determined and compared with theoretical expectations. A partial cross-section estimate for $(\bar{b}\Lambda_b^o)$ associated production is derived. Finally the results[1] are compared with those relative to our previous ISR experiment (R415), where the first evidence for Λ_b^o production was obtained with a smaller solid-angle for lepton detection and a lower integrated luminosity [2] [3].

---

[1] Already presented elsewhere in a preliminary version [1].

2. SET-UP

The set-up used in R422 experiment has already been described elsewhere [4]. This consisted of the SFM (Split Field Magnet) charged-particle spectrometer, shown in fig.1, equipped, in the 90° regions with respect to the beam axis, with two powerful electron (positron) detectors.

The system of multi-wire proportional chambers (MWPC, in fig.1) surrounding the interaction region [5], coupled to the SFM magnet (~1 Tesla), allowed charged track reconstruction over about 90 % of the total solid-angle. More than 75 % of reconstructed tracks had $\Delta p/p<30$ %.

An auxiliary time-of-flight system (TOF, in fig.1), made of scintillator counter hodoscopes [6], provided π/K/p separation over about 10 % of the total solid-angle for momenta below ~1GeV/c.

Each electron (positron) detector consisted of the following elements.

- Two electromagnetic shower calorimeters to require a minimum energy release $E>0.5$ GeV, at the trigger level. These calorimeters are indicated in fig.1 as LST2, LST5 on the so-called β^+ side (in the direction of the pp centre-of-mass motion), and SW3, SW4 on the β^- side. The SW-type calorimeters [7] were made of lead/scintillator plates, with 4×2 m^2 total area, 8 X_o, $\sigma(E)/E\cong(15\ \%)/\sqrt{E}$. In the LST-type calorimeters, the scintillator was replaced by planes of limited-streamer-tubes [8], with 4.6×2.4 m^2 total area, 7.5 X_o, $\sigma(E)/E\cong(20\div30)$ % for $0.5<E<4$ GeV. The charged pion detection efficiency, measured in test runs for both kinds of calorimeters, was of the order of 10^{-2} in the SW-type calorimeters and 10^{-3} in the LST-type, for an electron efficiency of about 90 % at E=1 GeV.

- Three Cherenkov counters [9] (C1, C2, C5 on the β^+ side and C0, C3, C4 on the β^-, as shown in fig.1). These were Nitrogen filled and also used in the electronic trigger logic via twofold coincidences to improve the electron/hadron separation achieved by the calorimeters.

- A small wire chamber [10] (DE/DX 109 on the β^+ side, DE/DX 209 on the β^-, see fig.1) with analogue read-out, which entirely covered the $e^-(e^+)$ trigger region (defined by Cherenkov counters plus calorimeters) and which allowed the identification and rejection at the off-line software level of the unwanted background of narrow e^+e^- pairs. These were mainly due to neutral hadron decays and photon conversions.

The acceptance of the apparatus for $e^{\pm}$ detection was $\sim 1.95\times10^{-2}$ on the β^+ side, and $\sim 1.2\times10^{-2}$ on the β^- side.

3. DATA TAKING AND FILTERING

The total number of collected events by means of the 90° single electron (positron) trigger was 3.3×10^7, corresponding to an integrated luminosity $L=1.27\times10^{37}\ cm^{-2}$. The data were submitted to a refined $e^{\pm}$ filtering analysis whose reduction power was of the order of 10^{-2}. For details about the analysis procedure, we refer the reader to ref.4. Let us just recall a few points.

- The $e^{\pm}$ track was first reconstructed in the 90° region and the electronic trigger requirements were again applied in a more stringent way to the calorimeter and Cherenkov responses. In particular, the energy measurement in the calorimeter was required to match the momentum measurement in the magnetic field.

- This track was then analysed with respect to the traversed DE/DX chamber. Here a drastic reduction of the background of e^+e^- pairs, due to external γ conversions (in the beam-pipe wall or in the front face of the DE/DX chamber itself) and to π^o, η, Dalitz decays, was achieved.

- The events surviving the off-line filter were fully reconstructed and the $e^{\pm}$ track was required to originate from the common event vertex. In more than 99 % of the events, only one trigger track was present and satisfied all the conditions imposed.

The background level in the remaining sample of 4.5×10^5 $e^{\pm}$ triggers was estimated from calibration runs and Monte Carlo studies. About 50 % of the final leptons were still due to lepton pair contamination and to known sources such as Compton effect or K_{l3} decay [9], while the residual contribution from charged hadrons was at the few percent level. Hence the (genuine $e^{\pm}$)/(background $e^{\pm}$) ratio was approximately 1:1. The overall lepton detection efficiency was (0.28 ± 0.05) for $p_t\geq1$ GeV/c, taking into account both the on-line trigger and the off-line analysis. The same quantity for charged hadrons was instead $\sim 1.5\times10^{-5}$.

4. INVARIANT MASS ANALYSIS

The invariant mass analysis was based on the identification of at least one of the charged particles participating in the multibody hadronic decay of the heavy-flavoured state searched for. This in order to avoid a prohibitive combinatorial background which would arise from the high charged-particle multiplicity (~16 on the average) of the $e^{\pm}$ triggered pp final states.

In about half of the cases a proton is present among the decay products of a heavy baryon and, in pp interactions, the proton is indeed the best candidate for identification. By taking advantage of the proton "leading" effect [11], i.e. of its property to carry away a considerable fraction (~50 % on the average) of the incident proton longitudinal momentum even in non-elastic, non-diffractive events, this proton could be simply selected as a positive-charge particle having a Feynman-x_F value (where $x_F=2|p_L|/\sqrt{s}$, p_L being the momentum component along the y-axis, see fig.1) above a given threshold value. This value was chosen in such a way as to optimize the proton detection efficiency and to minimize at the same time the π^+ contamination, which could be evaluated according to the experimentally measured p/π^+ ratio as a function of x_F in pp collisions [12]. This ratio increases exponentially as x_F increases and is already at the 1.5 level for $x_F=0.3$, the threshold used in the present analysis. About 20 % of the selected events contained a "leading" proton.

The "leading" effect, related to the quantum number flow from the initial to the final state particles [11], also applies to heavier baryons such as the Λ_s^o [13] and the Λ_c^+ [4] and manifests itself by a rather flat x_F production distribution of the type $(1-x_F)^n$, with $n=1\div2$. This suggested that even a heavier baryon could follow a similar production trend. Hence a "leading" condition could be important in the search for Λ_b^o in the "forward" region.

Turning now to the associated antibeauty decay generating the e^+, a relatively high p_t cut was imposed on the positron. In fact a massive open-flavoured state is predicted to be produced with an exponentially falling transverse momentum distribution having a mean value of the order of m_q [14] [15] (where m_q is the quark mass). This consequently affects the decay lepton spectrum. For charm states, a high p_t production distribution of the type $(1/p_t)dN/dp_t \propto \exp(-2.5p_t)$ has been indeed experimentally found [4] [16], and an even higher p_t distribution is therefore expected for a beauty state. The value of the $p_t(e^+)$ cut, i.e. 800 MeV/c, was chosen so as to avoid a too severe reduction of the data sample.

For "leading" baryon plus high p_t lepton selection, precise conditions were imposed

on the particles participating in reaction (1) via either the 4-body decay (2) or the 6-body decay (3). The efficiency of such an approach has already been tested in the past R415 experiment, where the first evidence for Λ_b^o production was found [2].

4.1 The $[p(K^-\pi^+)\pi^-]$ invariant mass

The motivations for the choice of the $(pD^o\,\pi^-)$ decay channel, with $D^o \rightarrow K^-\pi^+$, have already been given elsewhere [2]. However it is worthwhile repeating that, due to the baryonic and beauty-flavoured nature of the state which was searched for in this analysis, the presence of a proton together with a charmed meson among its decay products was favoured.

Four-body $[p(K^-\pi^+)\pi^-]$ combinations were selected in events where an e^+ was present with a transverse momentum $p_t>0.8$ GeV/c and a momentum uncertainty $\Delta p/p<15$ %. This second condition was imposed to avoid any charge sign ambiguity very close to the x-axis (see fig.1), where the SFM magnetic analysis was weak. All these four particles, plus the positron, had to originate from the reconstructed event vertex within ±5 cm.

The proton was defined to be the fastest positive-charge particle with $x_F>0.3$ and $\Delta p/p<8$ %. In this case the momentum error cut guarantees good accuracy for the highest momentum value involved in the invariant mass calculation.

The K^-, π^+ and π^- were any three charged particles of the event with $\Delta p/p<30$ % and not identified by the TOF system as π^- or $\bar{p}$ in the K^- case, as K^+ or p in the π^+ case, as K^- or $\bar{p}$ in the π^- case. These vetoing criteria only acted at the few percent level, given the small TOF acceptance for particle identification, as already mentioned in section 2. However they contributed to the reduction of the combinatorial background level. For the π^+, obviously $x_F<0.3$ was required.

The 4-body combinations selected in this way were then submitted to the following conditions.

- To have a rapidity $Y(4\text{-body})>1.4$, where $Y=0.5\ \ln[(E+|p_L|)/(E-|p_L|)]$. This condition, coupled to the "leading" proton identification method, was used to enhance the expected "forward" baryon yield. In fact the phase-space region selected in this way was $x_F(4\text{-body})>0.35$.

- To include at least one particle (among those selected as K^-, π^+ and π^-) belonging to the opposite hemisphere, with respect to the proton, i.e. such that

$p_L(p) \times p_L(particle) < 0$. This requirement, corresponding to the involvement of large angles in the 4-body invariant mass, was intended to enrich the sample selected in the higher mass region.

- To be correlated to a resonant $(K^-\pi^+)$ charm contribution from the D^o meson. This was achieved by operating a scan of the $(K^-\pi^+)$ invariant mass spectrum by intervals, 150 MeV/c^2 wide, in the neighbourhood of the D^o nominal mass.

Figure 2 shows the invariant mass lego-plot of $m(K^-\pi^+)$ versus $m[p(K^-\pi^+)\pi^-]$, for e^+ triggered events. An enhancement is visible for $1.90 \leq m(K^-\pi^+) < 2.05$ GeV/c^2 and $5.55 \leq m[p(K^-\pi^+)\pi^-] < 5.75$ GeV/c^2. The projection on the $m[p(K^-\pi^+)\pi^-]$ axis is presented in fig.s 3a and 3b, where the invariant mass spectra of the $[p(K^-\pi^+)\pi^-]$ combinations obtained in the presence of an e^+ trigger are shown in two cases:

a) $1.90 \leq m(K^-\pi^+) < 2.05$ GeV/c^2

b) $1.75 \leq m(K^-\pi^+) < 1.90$ GeV/c^2 or $2.05 \leq m(K^-\pi^+) < 2.20$ GeV/c^2.

The same spectra, corresponding to e^- triggers, are superimposed in fig.s 3a and 3b (dashed-line histograms) after normalization to the number of entries belonging to the mass regions below and above a 600 MeV/c^2 wide interval around ~5.5 GeV/c^2. A clear signal is visible in fig.3a for e^+ only, not for e^-. The spectra of fig.3a and 3b, relative to e^+, are also shown after normalization in fig.4, where the full-line histogram refers to the above selection a) and the dashed-line one to selection b). Here again the signal corresponding to selection a) is clearly visible. Hence either the e^- triggered spectrum of fig.3a or the e^+ triggered spectrum of fig.3b can be used to provide the background shape. In fact both these spectra have been checked to be well in agreement with the "event mixing" method (using particles from different events) to compute the invariant mass.

After background subtraction, the signal corresponds to (55.0±19.5) mass combinations in fig.3a and to (52.0±18.5) mass combinations in fig.4, in the region (5.55÷5.75) GeV/c^2. Its statistical significance is at the 3σ level. These numbers have been obtained by first parametrizing the polynomial shape of the above-quoted background spectra (dashed-line histograms of fig.s 3a and 4). Then a fit of the e^+ induced spectrum containing the signal (full-line histogram in fig.3a or fig.4) was made using the background polynomial curve plus a gaussian curve. The areas of the two curves, together with the peak position and standard deviation of the gaussian curve, were introduced as fit parameters.

It should be noticed that a signal can also in principle be observable in the spectrum

corresponding to e^-, if the antibeauty state decays hadronically into an anticharm state, which in turn decays semileptonically into an antistrange state via the emission of a W^- giving an $\bar{\nu}e^-$ pair. However, due to the $\bar{b} \rightarrow \bar{c} \rightarrow \bar{s}$ double decay chain, the p_t spectrum of the e^- would be degraded with respect to the same spectrum relative to e^+ from the direct $\bar{b}$ decay. Therefore a beauty signal associated to an e^- with $p_t > 0.8$ GeV/c would be depressed by almost a factor of 10 with respect to the corresponding e^+ triggered signal, as derived by Monte Carlo simulation. This is the reason why the invariant mass spectrum associated to e^- triggers has been taken as the background reference spectrum. Moreover, the fact that the signal of fig.3a disappears when the e^-, instead of the e^+, is selected, is a further argument to support its interpretation as a genuine beauty baryon effect.

The $(K^-\pi^+)$ mass interval (1.90÷2.05) GeV/c^2, correlated to the 4-body signal (fig.2), is centred around 1.975 GeV/c^2. This value is shifted upwards by 110 MeV/c^2 with respect to the nominal D^o mass (1.865 GeV/c^2). However this interval corresponds to the maximum effect in the 4-body invariant mass when scanning the $(K^-\pi^+)$ spectrum in the D meson mass range. Moreover this effect is only visible in the presence of e^+, as expected for charm from beauty decay (a charm signal from direct $c\bar{c}$ production would be associated to e^- from $\bar{c} \rightarrow e^-X$ decay).

A comment is now in order. The SFM apparatus, when used in heavy flavour searches as an invariant mass spectrometer, has always shown to be inadequate for precise mass measurements. Upward or downward mass shifts at the few percent level have been observed in the detection of charm states, D mesons and Λ_c^+ baryon, both in the past R415 [2] [17] [18] [19] and in the present R422 [4] experiments. Such shifts have been attributed to the fact that the SFM apparatus was only made of separate, movable elements (about 60 individual wire chambers) installed in a highly inhomogeneous magnetic field. Field mapping and alignment problems could be responsible for local systematic effects (both on angles and momenta). And these are at the origin of shifts in the invariant mass measurements. It is therefore not surprising that the D^o mass, as measured in the present analysis, happens to be shifted by about 6 % above its nominal value.

Having these arguments in mind, the signal in the $[p(K^-\pi^+)\pi^-]$ invariant mass spectrum of fig.3a or fig.4 can definitely be interpreted as a $(pD^o\pi^-)$ state, the Λ_b^o beauty baryon, decaying into charm in the presence of an e^+ originated by the associated $\bar{b}$ state.

The width of the Λ_b^o peak, ~200 MeV/c^2, is compatible with the expected mass resolution. The combinations/event ratio in the interval where the peak is observed is ~1.3. The Λ_b^o mass value estimate is derived from the previously mentioned fit of the e^+ triggered

spectrum of fig.3a or fig.4. Once the shift on the D^o mass is taken into account, the Λ_b^o mass is estimated to be:

$$m(\Lambda_b^o) = (5.64 +0.10 -0.21)\ GeV/c^2.$$

This value agrees within few percents with the one previously measured in similar conditions and through the identical decay channel in R415 experiment [2], i.e. (5.425 +0.175 -0.075) GeV/c^2. Notice that in this case the Λ_b^o signal was associated to a D^o mass shifted downwards by 100 MeV/c^2.

4.2 The $[(pK^-\pi^+)\pi^+\pi^-\pi^-]$ invariant mass

Since the Λ_b^o baryon is Cabibbo-favoured to decay into charm, it was quite natural to explore decay channels involving also the charmed baryon Λ_c^+. The $(\Lambda_c^+\pi^+\pi^-\pi^-)$ decay was preferred to the $(\Lambda_c^+\pi^-)$ one, since it allows to reach a much higher acceptance in the (5÷6) GeV/c^2 mass range. Concerning the Λ_c^+ decay mode, $\Lambda_c^+ \rightarrow pK^-\pi^+$ was searched for. Such a decay channel has already been successfully studied both in R422 [4] and R415 [19] experiments. The final choice was therefore the 6-body $[(pK^-\pi^+)\pi^+\pi^-\pi^-]$ combination.

All particles were selected as described in section 4.1 for the 4-body decay. Further conditions were imposed on the 6-body system.

- To belong to very high multiplicity events, i.e. with $n_{ch}>12$, where n_{ch} is the multiplicity of charged tracks associated to the vertex within ±5 cm, with $\Delta p/p<30$ %. This requirement was motivated by the non negligible multiplicity of the decay system itself.

- To be related to some "activity" in the opposite hemisphere. This condition was realized by demanding $0.25<(x_F)_{opp}<0.65$, where $(x_F)_{opp}=\Sigma_i x_F(i)$ and the index i runs over all particles (associated to the vertex, with $\Delta p/p<30$ %) having $p_L(i)\times p_L(6\text{-body})<0$.

- To have a rapidity Y(6-body)>1.7. Here again "leading" conditions were required.

- To correspond to a resonant $(pK^-\pi^+)$ charm system. The charm decay particles were required to belong to the same hemisphere, i.e. $p_L(p)\times p_L(K^-)>0$ and $p_L(p)\times p_L(\pi^+)>0$, and here again a scan was made of the $m(pK^-\pi^+)$ spectrum, by 200 MeV/c^2 wide intervals, around the Λ_c^+ nominal mass value.

A 6-body invariant mass spectrum is obviously affected by a huge combinatorial background. Hence the analysis was performed with a maximum number of allowed 6-body combinations, per event and per mass bin (150 MeV/c^2 wide), equal to 12.

The resulting $[(pK^-\pi^+)\pi^+\pi^-\pi^-]$ invariant mass spectra (fig.s 5a and 5b) correspond to the selections:

a) $2.23 \leq m(pK^-\pi^+) < 2.43$ GeV/c^2

b) $2.03 \leq m(pK^-\pi^+) < 2.23$ GeV/c^2 or $2.43 \leq m(pK^-\pi^+) < 2.63$ GeV/c^2

with e^+ triggers. The normalized background spectra superimposed in fig.s 5a and 5b (dashed-line histograms) are again provided by the e^- triggered event sample. In fig.5a a peak of (90±21) combinations shows up in the mass interval (5.5÷5.8) GeV/c^2. The combinations/event ratio in this mass interval is about 2.5, a value higher than in the previous case (see section 4.1) due to the increased decay multiplicity. The peak width is ~300 MeV/c^2. The statistical significance is ~4σ. The amplitude, mass, and width of the signal have been derived by a fit of the e^+ induced spectrum of fig.5a, as described in section 4.1.

The signal is only visible for $m(pK^-\pi^+)$ values in the mass bin (2.23÷2.43) GeV/c^2 which contains the Λ_c^+ nominal mass value, i.e. 2.285 GeV/c^2. It should be noticed that, in this case also, the central value of this bin, 2.33 GeV/c^2, is shifted upwards by 45 MeV/c^2 with respect to the nominal charm mass value.

The mass of the signal in fig.5a, once the Λ_c^+ mass shift is taken into account, can be quoted as:

$$m(\Lambda_b^o) = (5.65 +0.15 -0.20) \text{ GeV}/c^2$$

in excellent agreement with the mass value derived by means of the D^o decay channel (section 4.1). Notice that in both cases there is an upward systematic shift of the charm mass involved.

Due to its characteristics, the 6-body signal of fig.5a can again be interpreted as evidence for the observation of the Λ_b^o in a different decay channel.

4.3 The Λ_b^o mass

Figure 6 contains a summary of the experimental and theoretical status concerning the Λ_b^o mass estimate. Five theoretical predictions obtained in the framework of potential

models [20] are reported, together with their corresponding lower and upper bounds (vertical lines). All these predictions converge towards a value of ~5.6 GeV/c^2. A sixth theoretical value, obtained with scalar lattice QCD calculations [21], is also shown in fig.6. However it strongly disagrees both with the previously quoted theoretical estimates and with the experimental measurements. The average value relative to the three experimental (R415 and R422) measurements is:

$$m(\Lambda_b^o) = (5.57 +0.23 -0.22)\ GeV/c^2.$$

The quoted errors correspond to the lower and upper error-bar limits of the experimental points in fig.6. This mass value has to be compared with the corresponding theoretical average (computed using the five potential model estimates only):

$$m(\Lambda_b^o) = (5.59 +0.07 -0.21)\ GeV/c^2.$$

In this case the errors are derived from the theoretical lower and upper bounds reported in fig.6.

From these numbers one can conclude that there is a very good agreement between experiment and theory.

5. CROSS-SECTION ESTIMATE

It is difficult, from the number of observed events, to estimate a total cross-section value for ($\bar{b}\Lambda_b^o$) associated production. In fact the fraction of solid-angle covered by our detector was of the order of 10^{-2}, essentially because of the $e^{\pm}$ telescopes (see section 2). The results obtained in such a limited solid-angle by the selective analysis described so far, can only be extrapolated using a model-dependent Monte Carlo simulation where very many hypotheses have to be made. These concern:

- the nature (baryonic or mesonic, ground or excited) of the $\bar{b}$ state;
- the transverse and longitudinal production distributions of the Λ_b^o;
- the transverse and longitudinal production distributions of the $\bar{b}$ state;
- the correlation existing between the two produced states;
- the mechanism of the Λ_b^o hadronic decay;
- the mechanism of the D^o (or Λ_c^+) hadronic decay;

- the mechanism of the $\bar{b}$ state semileptonic decay.

Moreover, three decay branching ratios are needed, one of them being unknown.

Therefore we have considered a partial cross-section, namely the so called "visible" cross-section. This is defined as:

$$\sigma_{vis} = N/(\varepsilon \times L \times \Pi_{BR})$$

where N is the number of observed events, ε the overall detection efficiency, L the luminosity and Π_{BR} the product of all decay branching ratios involved. This quantity represents the experimental lower limit of the total cross-section. In the present exercise, we have considered only the $\Lambda_b^o \rightarrow pD^o\pi^-$ decay mode (2), because of its lower combinatorial background level, compared to the decay mode (3). Of course the final result will be σ_{vis} times the unknown Λ_b^o decay branching ratio.

The number of events N is derived dividing by 1.3 the number of observed Λ_b^o invariant mass combinations (see section 4.1). The luminosity is $L=1.27\times10^{37}$ cm^{-2}. The overall efficiency for detecting the $(e^+pK^-\pi^+\pi^-)$ system is $\varepsilon=\varepsilon(e^+)\times\varepsilon(pK^-\pi^+\pi^-)$, with $\varepsilon(e^+)=(26\pm5)$ % for $p_t(e^+)>0.8$ GeV/c, and $\varepsilon(pK^-\pi^+\pi^-)=(19\pm4)$ %. The branching ratios involved refer to $D^o \rightarrow K^-\pi^+$ and $\bar{b} \rightarrow e^+X$ decays. For the first one, we have taken $BR(D^o \rightarrow K^-\pi^+)=(3.71\pm0.25)$ % [22]. For the second one, we have made the assumption that the $\bar{b}$ state is an antimeson, with $BR(\bar{b} \rightarrow e^+X)=BR(B^\pm, B^o, \bar{B}^o \rightarrow e^\pm X)=(12.1\pm0.6)$ % [22]. The "visible" cross-section, times the branching ratio, turns out to be:

$$BR(\Lambda_b^o \rightarrow pD^o\pi^-)\times\sigma_{vis}(\bar{b}\Lambda_b^o) = (14\pm6) \text{ nb.}$$

The above number indicates what the cross-section would be if the whole $(\bar{b}\Lambda_b^o)$ production occurred in the phase-space region defined by the solid-angle coverage of the apparatus and by the additional cuts introduced in the analysis. This number is compatible, within the experimental errors, with our previous R415 result [3], once the difference in solid-angle for $e^\pm$ detection is duly taken into account.

6. CONCLUSIONS

The main point of the present work is the observation of the lowest baryonic open-beauty state, Λ_b^o, via another decay mode (3). This confirms the results of our previous

experiment, R415, where the Λ_b^o was observed via the decay mode (2), also seen in the present experiment. The Λ_b^o is again observed in the "leading" part of the phase-space, i.e. in the high x_F region ($x_F>0.35$). Its mass, averaged over R422 and R415 measurements, is found to be $m(\Lambda_b^o)\cong 5.6$ GeV/c^2, in good agreement with theoretical predictions.

ACKNOWLEDGEMENTS

We are thankful to A. Martin and J.M. Richard for their interest in our work and for useful discussions. We also acknowledge the co-operation of the ISR Experimental Support Group and the SFM Detector Group. Finally we are grateful to our technicians, J. Berbiers, H. Bienkowsky, Y. Cholley, D. Fabbri, F. Massera, G. Molinari, R. Pilastrini and M. Ventura, for their skilful work during the preparation, assembly and running stages of the experiment.

REFERENCES

[1] L. Cifarelli.
Proc. of the 2nd San Miniato Topical Seminar on Heavy Flavours (Ed. F.L. Navarria), Nucl. Phys. (Proc. Suppl.) 1B, 55 (1988).

[2] M. Basile, G. Bonvicini, G. Cara Romeo, L. Cifarelli, A. Contin, G. D'Alì, P. Di Cesare, B. Esposito, P. Giusti, T. Massam, R. Nania, F. Palmonari, G. Sartorelli, G. Valenti and A. Zichichi.
Nuovo Cimento Lett. 31, 97 (1981).

[3] M. Basile, G. Bonvicini, G. Cara Romeo, L. Cifarelli, A. Contin, G. D'Alì, P. Di Cesare, B. Esposito, P. Giusti, T. Massam, R. Nania, F. Palmonari, G. Sartorelli, G. Valenti and A. Zichichi.
Nuovo Cimento 65A, 391 (1981).

[4] G. Bari, M. Basile, G. Bruni, G. Cara Romeo, R. Casaccia, L. Cifarelli, F. Cindolo, A. Contin, G. D'Alì, C. Del Papa, S. De Pasquale, P.Giusti, G. Iacobucci, G. Maccarrone, T. Massam, R. Nania, F. Palmonari, G. Sartorelli, G. Susinno, L. Votano and A. Zichichi.
Nuovo Cimento 104A, 571 (1991).

[5] a) R. Bouclier, G. Charpak, E. Chesi, L. Dumps, H.G. Fischer, H.J. Hilke, P.G. Innocenti, G. Maurin, A. Minten, L. Naumann, F. Piuz, J.C. Santiard and O. Ullaland.
Nucl. Instr. and Meth. 115, 235 (1974).
b) R. Bouclier, R.C.A. Brown, E. Chesi, L. Dumps, H.G. Fischer, P.G. Innocenti, G. Maurin, A. Minten, L. Naumann, F. Piuz and O. Ullaland.
Nucl. Instr. and Meth. 125, 19 (1975).

[6] M. Basile, G. Cara Romeo, L. Cifarelli, A. Contin, G. D'Alì, P. Di Cesare, B. Esposito, L. Favale, P. Giusti, T. Massam, F. Palmonari, G. Sartorelli, G. Valenti and A. Zichichi.
Nucl. Instr. and Meth. 179, 477 (1981).

[7] M. Basile, G. Cara Romeo, L. Cifarelli, A. Contin, G. D'Alì, F. Palmonari, G. Sartorelli, G. Valenti and A. Zichichi.
Nucl. Instr. and Meth. 163, 93 (1979).

[8] M. Basile, J. Berbiers, G. Bonvicini, G. Cara Romeo, L. Cifarelli, A. Contin, M. Curatolo, G. D'Alì, C. Del Papa, B. Esposito, D. Fabbri, P. Giusti, T. Massam, F. Massera, R. Nania, G. Natale, F. Palmonari, G. Sartorelli, M. Spinetti, G. Susinno, L. Votano and A. Zichichi.
Nucl. Instr. and Meth. A235, 74 (1985).

[9] M. Basile, G. Cara Romeo, L. Cifarelli, A. Contin, G. D'Alì, P. Di Cesare, B. Esposito, P. Giusti, T. Massam, F. Palmonari, G. Sartorelli, G. Valenti and A. Zichichi.
Nuovo Cimento 65A, 421 (1981).

[10] a) H. Frehse, F. Lapique, M. Panter and F. Piuz.
Nucl. Instr. and Meth. 156, 87 (1978).
b) H. Frehse, M. Heiden, M. Panter and F. Piuz.
Nucl. Instr. and Meth. 156, 97 (1978).

[11] M. Basile, G. Cara Romeo, L. Cifarelli, A. Contin, G. D'Alì, P. Di Cesare, B. Esposito, P. Giusti, T. Massam, R. Nania, F. Palmonari, V. Rossi, G. Sartorelli, M. Spinetti, G. Susinno,G. Valenti, L. Votano and A. Zichichi.
Nuovo Cimento 66A, 129 (1981).

[12] P. Capiluppi, G. Giacomelli, A.M. Rossi, G. Vannini and A. Bussière.
Nucl. Phys. 70B, 1 (1974).

[13] S. Erhan, W. Lockman, T. Meyer, J. Rander, P. Schlein, R. Webb and J. Zsembery.
Phys. Lett. 85B, 447 (1979).

[14} Y. Afek, C. Leroy and B. Margolis.
Phys. Rev. D22, 86 (1980).

[15] E. L. Berger.
Preprint ANL-HEP-PR-87-53 (1987).

[16] M. Basile, G. Cara Romeo, L. Cifarelli, A. Contin, G. D'Alì, P. Di Cesare, B. Esposito, P. Giusti, T. Massam, R. Nania, F. Palmonari, G. Sartorelli, G. Valenti and A. Zichichi.
Nuovo Cimento Lett. 33, 17 (1982).

[17] M. Basile, G. Cara Romeo, L. Cifarelli, A. Contin, G. D'Alì, P. Di Cesare, B. Esposito, P. Giusti, T. Massam, R. Nania, F. Palmonari, G. Sartorelli, G. Valenti and A. Zichichi.
Nuovo Cimento 65A, 457 (1981).

[18] M. Basile, G. Cara Romeo, L. Cifarelli, A. Contin, G. D'Alì, P. Di Cesare, B. Esposito, P. Giusti, T. Massam, R. Nania, F. Palmonari, G. Sartorelli, G. Valenti and A. Zichichi.
Nuovo Cimento 67A, 40 (1982).

[19] M. Basile, G. Cara Romeo, L. Cifarelli, A. Contin, G. D'Alì, P. Di Cesare, B. Esposito, P. Giusti, T. Massam, R. Nania, F. Palmonari, G. Sartorelli, G. Valenti and A. Zichichi.
Nuovo Cimento 63A, 230 (1981).

[20] A. Martin and J.M. Richard.
Preprint CERN-TH-4584/86 (1986) and references therein.

[21] S. Samuel and K.J.M. Moriarty.
Phys. Lett. 175B, 197 (1986).

[22] M. Aguilar Benitez et al. (Particle Data Group).
Phys. Lett. 239B (1990).

FIGURE CAPTIONS

Fig.1) The SFM spectrometer, top view:
MWPC: multi-wire proportional chambers;
DE/DX_i: multi-wire proportional chambers with analogue read-out (i=109, 209);
C_i: threshold Cherenkov counters (i=0, ..., 5);
TOF: time-of-flight scintillation counters;
SW_i: lead/scintillator-sandwich shower counters (i=3, 4);
LST_i: lead/limited-streamer tube shower counters (i=2, 5).
The x-y axes of the SFM reference system are shown.

Fig.2) Lego-plot of $(K^-\pi^+)$ invariant mass versus $[p(K^-\pi^+)\pi^-]$ invariant mass, obtained for e^+ triggers.

Fig.3) The $[p(K^-\pi^+)\pi^-]$ invariant mass spectra obtained for e^+ triggers (full-line histogram) and for e^- triggers (dashed-line histogram)
a) when $1.90 \leq m(K^-\pi^+) < 2.05$ GeV/c^2,
b) when $1.75 \leq m(K^-\pi^+) < 1.90$ GeV/c^2 or $2.05 \leq m(K^-\pi^+) < 2.20$ GeV/c^2.
The histograms corresponding to e^- are normalized to those corresponding to e^+ as explained in the text. The curves superimposed are polynomial fits of the dashed-line histograms.

Fig.4) The $[p(K^-\pi^+)\pi^-]$ invariant mass spectra of fig.s 3a and 3b, corresponding to e^+ triggers, superimposed after normalization. The full-line histogram is obtained for $m(K^-\pi^+)$ in the interval (1.90÷2.05) GeV/c^2, the dashed-line histogram for $m(K^-\pi^+)$ in the intervals (1.75÷1.90) GeV/c^2 and (2.05÷2.20) GeV/c^2. A fit to the latter is also shown.

Fig.5) The $[p(K^-\pi^+)\pi^+\pi^-\pi^-]$ invariant mass spectra obtained for e^+ triggers (full-line histogram)
a) when $2.23 \leq m(pK^-\pi^+) < 2.43$ GeV/c^2,
b) when $2.03 \leq m(pK^-\pi^+) < 2.23$ GeV/c^2 or $2.43 \leq m(pK^-\pi^+) < 2.63$ GeV/c^2.
The histograms corresponding to e^- are normalized to those corresponding to e^+.
The curves superimposed are polynomial fits of the dashed-line histograms.

Fig.6) The experimental values of the Λ_b^o mass, compared with the theoretical estimates given in ref.s 20 and 21:
■: experimental value derived via ($pD\pi$) decay;
□: experimental value derived via ($\Lambda_c\pi\pi\pi$) decay;
●: potential model estimate, as given in ref.20;
o: scalar lattice QCD estimate, as given in ref.21.
The theoretical lower and upper bounds for potential model estimates are indicated as vertical lines.

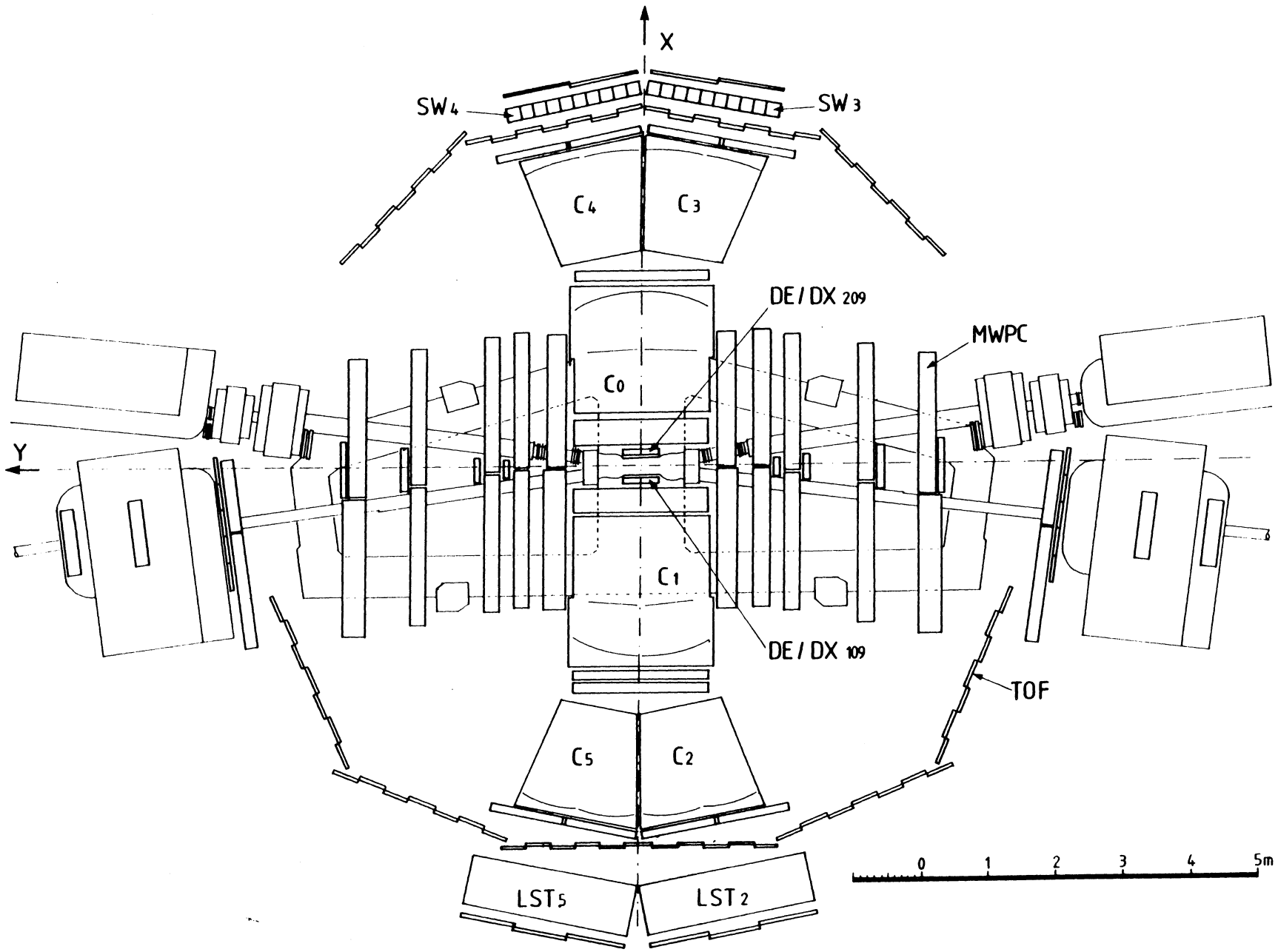
X
SW4
SW3
C4
C3
DE/DX 209
MWPC
C0
Y
C1
DE/DX 109
TOF
C5
C2
0
1
2
3
4
5m
LST5
LST2

Fig. 1

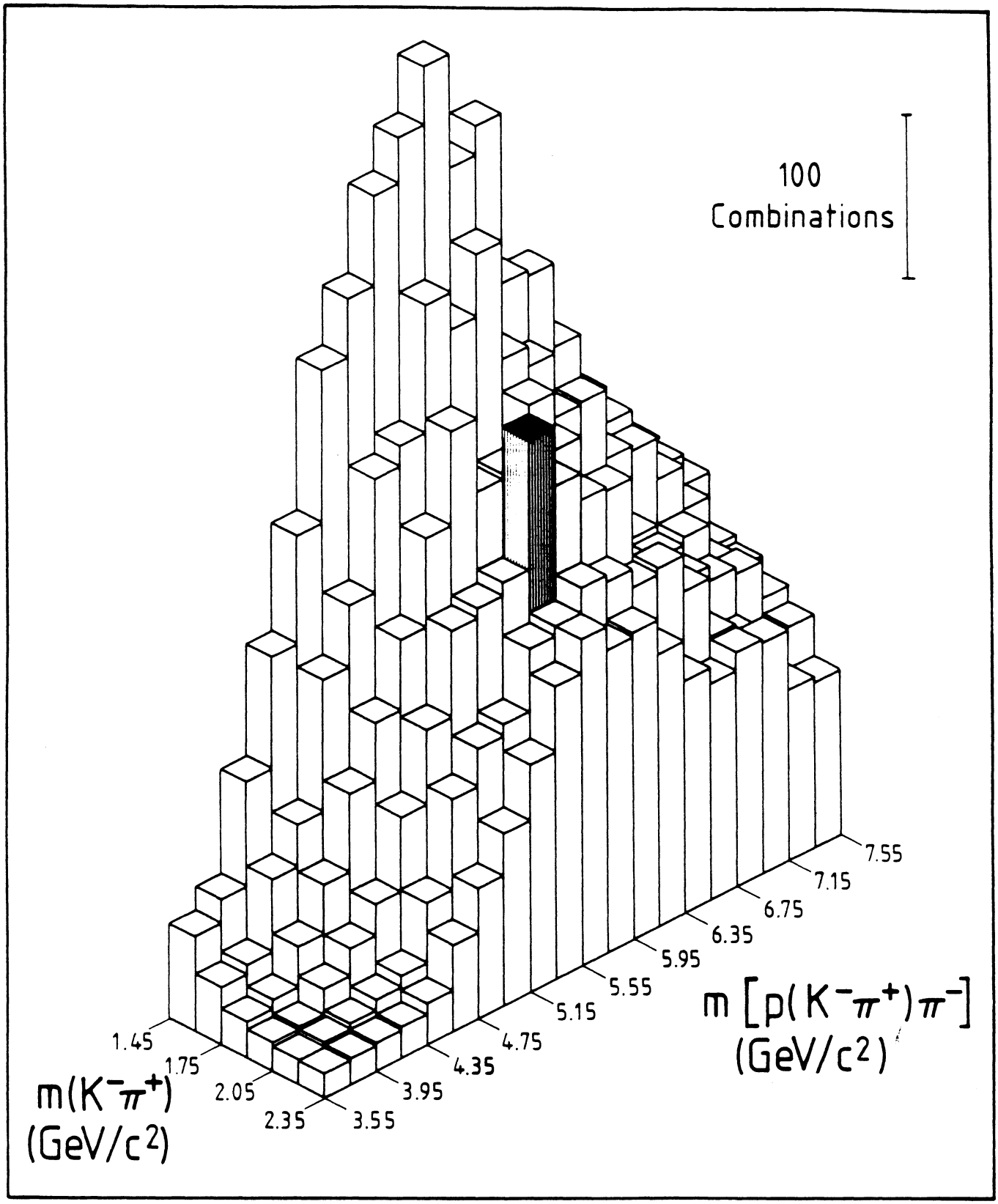
100
Combinations
m(K⁻π⁺)
(GeV/c²)
1.45
1.75
2.05
2.35
3.55
3.95
4.35
4.75
5.15
5.55
5.95
6.35
6.75
7.15
7.55
m [p(K⁻π⁺)π⁻]
(GeV/c²)

Fig. 2

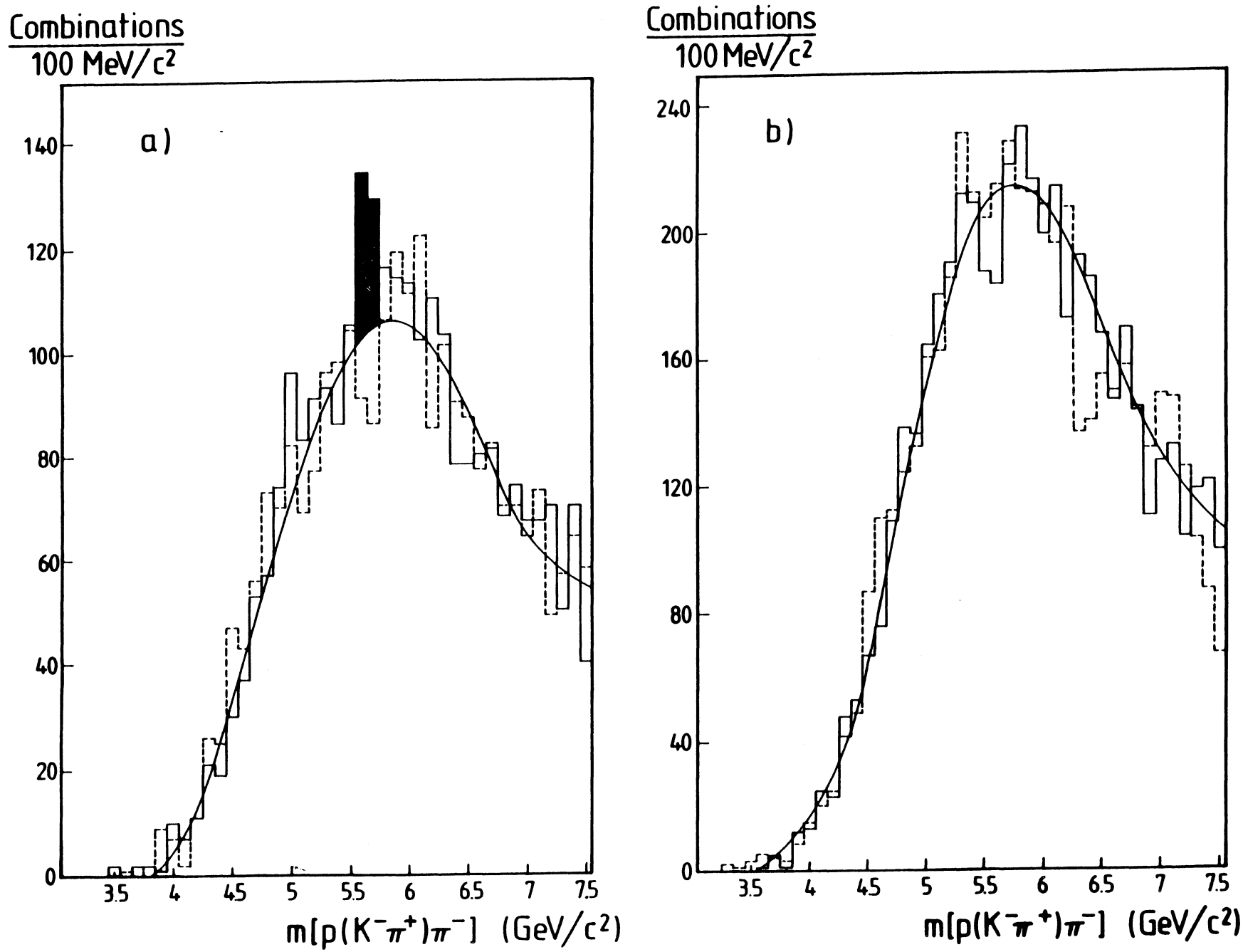
Combinations
100 MeV/c²
a)
140
120
100
80
60
40
20
0
3.5
4
4.5
5
5.5
6
6.5
7
7.5
m[p(K⁻π⁺)π⁻] (GeV/c²)
Combinations
100 MeV/c²
b)
240
200
160
120
80
40
0
3.5
4
4.5
5
5.5
6
6.5
7
7.5
m[p(K⁻π⁺)π⁻] (GeV/c²)

Fig. 3

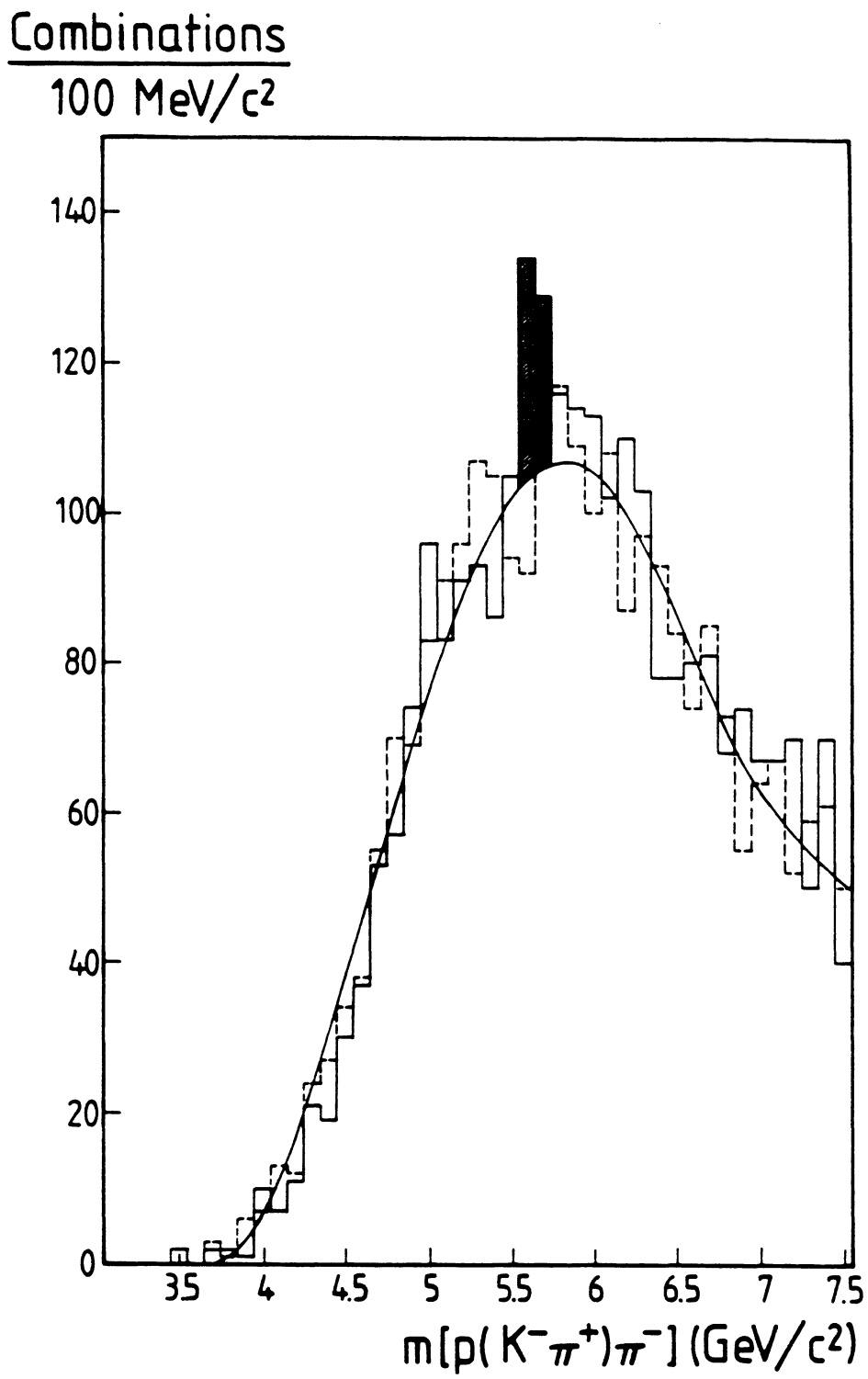
Combinations
100 MeV/c²
140
120
100
80
60
40
20
0
3.5
4
4.5
5
5.5
6
6.5
7
7.5
m[p(K⁻π⁺)π⁻] (GeV/c²)

Fig. 4

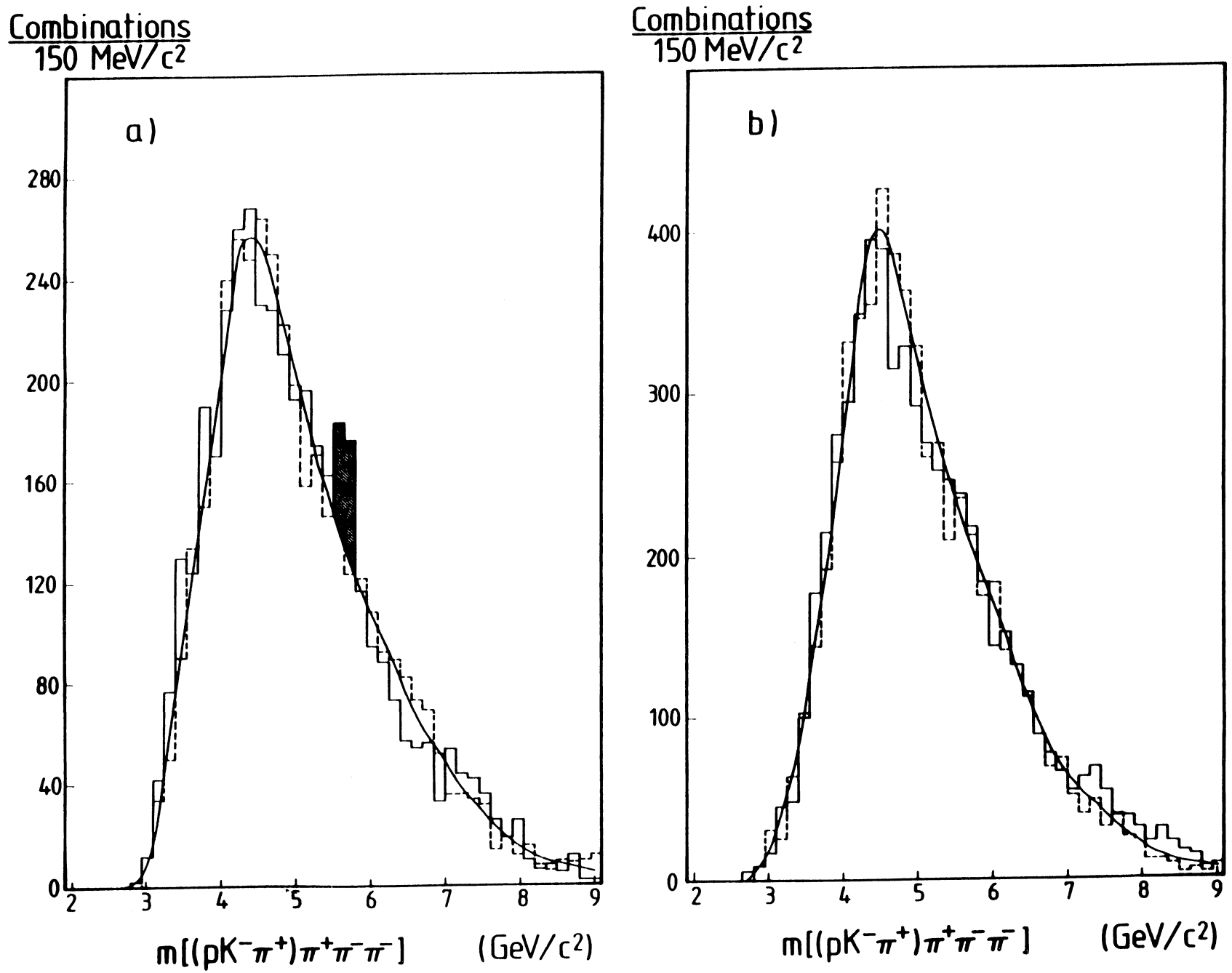
Combinations
150 MeV/c²
a)
280
240
200
160
120
80
40
0
2
3
4
5
6
7
8
9
m[(pK⁻π⁺)π⁺π⁻π⁻]
(GeV/c²)
Combinations
150 MeV/c²
b)
400
300
200
100
0
2
3
4
5
6
7
8
9
m[(pK⁻π⁺)π⁺π⁻π⁻]
(GeV/c²)

Fig. 5

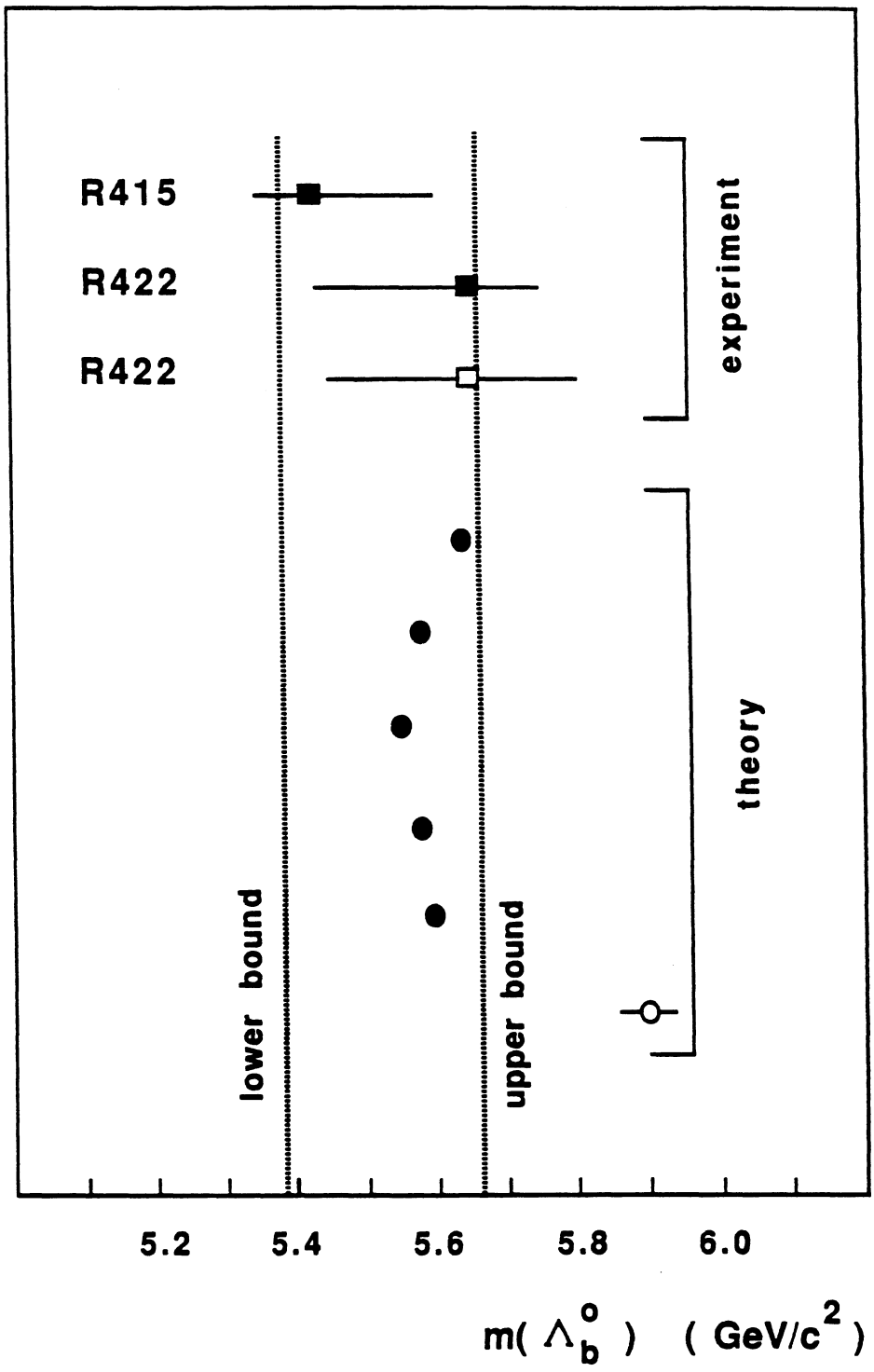
R415
R422
R422
experiment
theory
lower bound
upper bound
5.2
5.4
5.6
5.8
6.0
m(Λ_b^o) (GeV/c^2)

Fig. 6